

Ca–Mg diffusion in diopside: tracer and chemical inter-diffusion coefficients

Xiaoyu Zhang · Jibamitra Ganguly ·
Motoo Ito

Received: 20 March 2009 / Accepted: 8 July 2009 / Published online: 2 August 2009
© Springer-Verlag 2009

Abstract We have experimentally determined the tracer diffusion coefficients (D^*) of ^{44}Ca and ^{26}Mg in a natural diopside ($\sim\text{Di}_{96}$) as function of crystallographic direction and temperature in the range of 950–1,150 °C at 1 bar and $f(\text{O}_2)$ corresponding to those of the WI buffer. The experimental data parallel to the a^* , b , and c crystallographic directions show significant diffusion anisotropy in the a – c and b – c planes, with the fastest diffusion being parallel to the c axis. With the exception of $\log D^*(^{26}\text{Mg})$ parallel to the a^* axis, the experimental data conform to the empirical diffusion “compensation relation”, converging to $\log D \sim -19.3 \text{ m}^2/\text{s}$ and $T \sim 1,155 \text{ °C}$. Our data do not show any change of diffusion mechanism within the temperature range of the experiments. Assuming that D^* varies roughly linearly as a function of angle with respect to the c axis in the a – c plane, at least within a limited domain of $\sim 20^\circ$ from the c -axis, our data do not suggest any significant difference between $D^*(\parallel c)$ and $D^*(\perp(001))$, the latter being the diffusion data required to model compositional zoning in the (001) augite exsolution lamellae in natural clinopyroxenes. Since the thermodynamic mixing property of Ca and Mg is highly nonideal, calculation of

chemical diffusion coefficient of Ca and Mg must take into account the effect of thermodynamic factor (TF) on diffusion coefficient. We calculate the dependence of the TF and the chemical interdiffusion coefficient, $D(\text{Ca–Mg})$, on composition in the diopside–clinoenstatite mixture, using the available data on mixing property in this binary system. Our $D^*(\text{Ca})$ values parallel to the c axis are about 1–1.5 log units larger than those Dimanov et al. (1996). Incorporating the effect of TF, the $D(\text{Ca–Mg})$ values calculated from our data at 1,100–1,200 °C is ~ 0.6 – 0.7 log unit greater than the experimental quasibinary $D((\text{Ca–Mg} + \text{Fe}))$ data of Fujino et al. (1990) at 1 bar, and ~ 0.6 log unit smaller than that of Brady and McCallister (1983) at 25 kb, 1,150 °C, if our data are normalized to 25 kb using activation volume (~ 4 and $\sim 6 \text{ cm}^3/\text{mol}$ for Mg and Ca diffusion, respectively) calculated from theoretical considerations.

Keywords Diffusion · Thermodynamic factor · Diopside · Euclites · Cooling rates

Introduction

Clinopyroxenes in both slowly cooled terrestrial and planetary samples often show compositional zoning of major divalent cations and exsolution lamellae (e.g. McCallum and O’Brien 1996; Schwartz and McCallum 2005). These features can be modeled to constrain the cooling histories of the host rocks, if the appropriate diffusion kinetic parameters of the divalent cations are known. The relatively coarse exsolution lamellae, in which compositional zoning could be measured, are typically parallel to (001) so that the diffusion direction during the growth of the lamellae is normal to the (001) direction, or at an angle of 16–18° to the c -axis. In addition, the coarsening of the

Communicated by T.L. Grove.

X. Zhang · J. Ganguly (✉)
Department of Geosciences, University of Arizona,
Tucson, AZ 95721, USA
e-mail: ganguly@email.arizona.edu

M. Ito
ARES, NASA Johnson Space Center,
Houston, TX 77058, USA

M. Ito
Lunar and Planetary Institute, 3600 Bay Area Boulevard,
Houston, TX 77058, USA

exsolution lamellae can also be modeled using the theory of Brady (1987) and the available data on lamellar coarsening kinetics (McCallister 1978; Nord and McCallister 1979; Nord and Gordon 1980) to provide complementary constraints on the cooling rates of the host rocks. Several workers, thus, have carried out experimental studies over approximately the past three decades to determine the diffusion parameters of the divalent cations in diopside.

Brady and McCallister (1983) determined the quasibinary chemical interdiffusion coefficient of Ca and (Mg + Fe) at 25 kb, 1,150–1,250 °C from kinetic experiments involving homogenization of fine scale (001) coherent pigeonite exsolution lamellae in a sub-calcic diopside megacryst from Mabuki kimberlite, Tanzania. (As discussed later, a chemical interdiffusion coefficient represents a product of a weighted average of tracer diffusion coefficients and a thermodynamic factor.) They presented their data as “average” (chemical) inter-diffusion coefficient, $\bar{D}(\text{Ca-Mg})$ (which, in fact is $\bar{D}(\text{Ca}-(\text{Mg} + \text{Fe}))$), at the annealing temperatures since the inter-diffusion coefficient must have varied as a function of composition during homogenization as a result of the strong deviation from thermodynamic ideality of mixing of the Ca and Mg components (e.g. Lindsley et al. 1981), as discussed later. Fujino et al. (1990) determined $\bar{D}(\text{Ca} - (\text{Mg} + \text{Fe}))$, from modeling the compositional profiles, as determined by analytical transmission electron microscopy (ATEM) in (001) pigeonite exsolution lamellae and augite host in a natural crystal that was annealed to promote coarsening of the lamellae at several temperatures between 1,000 and 1,200 °C at 1 bar pressure and controlled $f(\text{O}_2)$ conditions. Dimanov et al. (1996) determined tracer diffusion coefficient of Ca, using natural crystal, whereas Azough and Freer (2000) determined that of Fe^{2+} using both natural and synthetic (Fe-free) crystals. Preliminary experimental data for Ca and Mg tracer diffusion coefficients in natural diopside were also presented from our group (Stimpfl et al. 2003) and were used by Schwartz and McCallum (2005) to model the compositional zoning in (001) exsolution lamellae of augite in pigeonite host in unequilibrated eucrites. Miyamoto and Takeda (1994) and Miyamoto (1997) used the quasi-binary Ca-(Mg + Fe) inter-diffusion data of Fujino et al. (1990) to estimate the cooling rate (and from that the burial depth) of an eucrite on the basis of the compositional zoning in (001) exsolved lamellae in clinopyroxene.

Availability of the tracer diffusion coefficients of the diffusing species, $D^*(i)$, as function of crystallographic orientation, along with their thermodynamic mixing properties, permits flexibility in the modeling of compositional zoning as function of diffusion direction and composition. There are now adequate data (e.g. Lindsley et al. 1981; Ganguly and Saxena 1987) to evaluate thermodynamic

effect on the diffusion process. However, so far no data have been available for $D^*(\text{Mg})$ in clinopyroxene. The primary purpose of this work is the determination of $D^*(\text{Ca})$ and $D^*(\text{Mg})$ in natural diopside crystals as functions of crystallographic orientation and temperature, and to use these data and thermodynamic mixing properties of Ca and Mg to calculate the binary chemical interdiffusion coefficient.

Experimental and analytical methods

Sample preparation

Chips of a gem quality natural diopside crystal, $\sim \text{Di}_{96}$, were oriented in a 4-circle X-ray diffractometer and cut normal to a^* , b and c axial directions. Complete microprobe analysis of the crystal yields a formula $\text{Ca}_{0.96}\text{Na}_{0.02}\text{Mg}_{0.96}\text{Fe}_{0.05}\text{Mn}_{0.01}\text{Al}_{0.04}\text{Si}_{1.97}\text{O}_6$, and shows the crystal to be effectively homogeneous. The cut surfaces were ground and were polished down to 0.25 μm diamond powder and finally finished to a mirror polish by a combination of mechanical and chemical polishing using silica suspension on OP-chem cloth from Struers. The last step was intended to remove a very thin disturbed layer that usually develops very close to a crystal surface by the abrasive action of mechanical polishing. The polished wafers were pre-annealed for 1–2 days at or close to the conditions of the diffusion experiments in order to equilibrate the point defects to a condition that is the same as or close to the experimental condition, and also to anneal the surface defects that might have been generated by the polishing process.

The source materials for Ca and Mg tracer diffusion experiments were ^{44}Ca enriched CaO and ^{26}Mg rich MgO , respectively. A thin layer ($\sim 200\text{--}250 \text{ \AA}$) of a source material was deposited on the polished surface of a pre-annealed crystal by thermal evaporation under high-vacuum condition. Initially, we tried to use ^{44}Ca enriched finely powdered CaCO_3 as a source material for ^{44}Ca , but the powder kept on flying off the tungsten filament upon which it was deposited for thermal evaporation by resistive heating. The problem was solved by decarbonation and grain coarsening in a furnace prior to deposition on the tungsten filament.

Tracer diffusion experiments

All experiments were carried out in a computer controlled vertical gas-mixing furnace. The oxygen fugacity was controlled by a flowing mixture of CO and CO_2 and cross checked by a zirconia sensor. The furnace was pre-conditioned to the desired temperature and $f(\text{O}_2)$ condition of an experiment keeping the ends of the vertical ceramic tube

closed. The sample with a thin layer of diffusing material was quickly inserted from the top to the hot spot of the furnace, and the ends of the ceramic tube were completely sealed immediately thereafter. In order to minimize gas consumption, the gas mixture was forced to recirculate into the furnace and was vented out periodically through a pressure release valve. After the end of an experiment, the sample was quenched quickly by pulling it out of the furnace and cooling in air.

Time series experiments were carried out at 1,000 °C and $f(\text{O}_2)$ corresponding to that of the wüstite-iron (WI) buffer to check if the retrieved diffusion coefficients show any time dependence that would be indicative of effects from non-diffusive processes on the development of the concentration profiles. The results of the time series experiments are discussed below.

Measurement of diffusion profiles

The experimentally induced diffusion profiles of ^{44}Ca and ^{26}Mg were measured by depth profiling in Ion-probes at the University of Tokyo (Cameca ims-6f SIMS) and Arizona State University (Cameca ims-3f SIMS). The primary ion beam was mass filtered negative ^{16}O accelerated to 10 keV with a beam current of 30–80 nA, and was rastered over $\sim 125 \times 125$ to $175 \times 175 \mu\text{m}$ square area of the sample during analyses. By using mechanical aperture, only the secondary ions from the central segment of $\sim 60 \mu\text{m}$ diameter of the rastered area were collected during depth profiling. The electrostatic charging of a sample by the primary ion beam irradiation was virtually eliminated by depositing a thin film ($\sim 30 \text{ nm}$) of either Pd (Tokyo facility) or Au (ASU facility) on the sample surface prior to analysis. At the end of depth profiling a sample, the crater depth within the sample was measured by a Dektak surface profilometer that was calibrated against known standards. Assuming that each step in the depth profiling caused the same penetration into the sample, the step size was calculated by dividing the crater depth by the total number of steps. This assumption may not be valid for the sputtering of the primary ion beam within the thin film versus the crystal. However, the error due to the possible difference between the step size within the film and the crystal substrate should have negligible effect on the calculation of the step size because of the overwhelmingly large number of steps within the crystal relative to those within a thin film.

In addition to ^{44}Ca and ^{26}Mg , the spatial variation of several other non-diffusing species, namely ^{30}Si , ^{25}Mg , ^{42}Ca or ^{54}Fe , and ^{104}Pb or ^{197}Au , was also measured simultaneously during the sputtering process. A typical set of analytical data for an experiment designed to determine ^{26}Mg diffusion at 1,100 °C is shown in Fig. 1.

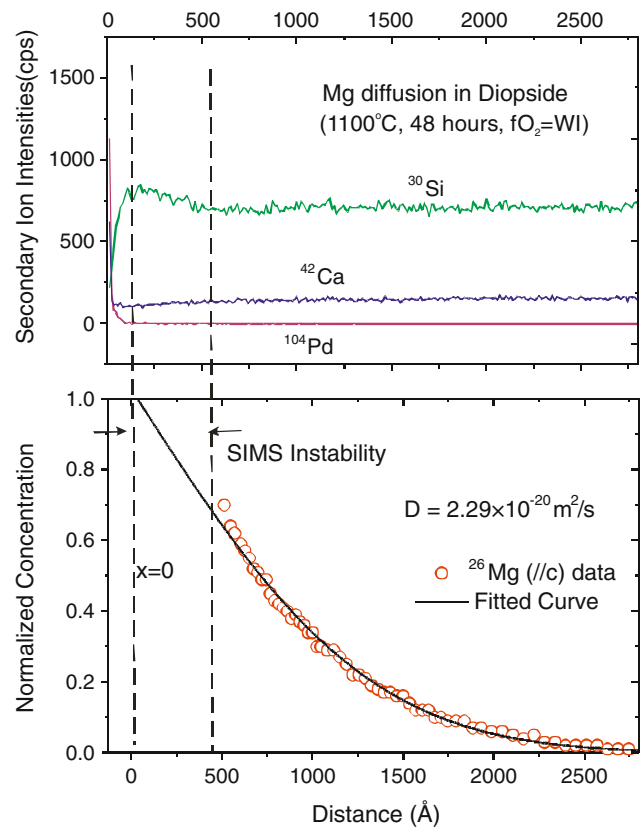


Fig. 1 A typical SIMS depth profile (*symbols*), showing the normalized concentration of ^{26}Mg versus penetration distance within the sample parallel to the c -axis of diopside, and the model fit to the data according to the solution of the diffusion equation (Eq. 1). Also shown are the depth profiles for the non-diffusing species ^{30}Si , ^{42}Ca and a surface layer of ^{104}Pd that was deposited to eliminate sample charging during SIMS analysis. The residual thin film surface is assumed to be located at half the intensity of ^{104}Pd , whereas the crystal surface ($x = 0$) is assumed to be located at the peak intensity of ^{30}Si

The concentration profiles of the non-diffusing species were used to locate the thin film and crystal surfaces. The mixing effect during depth profiling caused smearing out of the intensity of the Pd or Au layer over a certain distance. As in our previous studies, and for reasons discussed therein (e.g. Ganguly et al. 2007), it was assumed that the surface of a thin film was located approximately at half-intensity for the counts of ^{104}Pd or ^{197}Au , whereas the crystal surface was located at the initial peak of ^{30}Si (Fig. 1a). The criterion for locating the crystal surface is justified on the basis of an earlier study (Ganguly et al. 1998a) in which the diffusing species was deposited on the crystal surface from a dilute HCl solution. It was found that a sharp drop of Cl counts to almost zero value, which indicates a position at or very close to the crystal surface, coincided with the initial peak of ^{30}Si . It has been found in all our studies of diffusion kinetics involving Ion-probe analysis that the ^{30}Si counts attain a peak before settling to

a plateau value during depth profiling. We have also shown in Fig. 1 the profile of ^{42}Ca that is expected to be a non-diffusing isotope in the specific experiment. It should be noted that the crystal surface located on the basis of ^{30}Si peak approximately coincides with the beginning of plateau value of ^{42}Ca . A 50-Å uncertainty on the location of a crystal surface has negligible effect on the value of retrieved diffusion coefficients in our study in which the profile lengths were at least 1,200 Å.

Results and discussion

Modeling of the diffusion profiles

The experimentally produced diffusion profiles of ^{44}Ca and ^{26}Mg were modeled to retrieve the tracer diffusion coefficients according to the solution of diffusion equation in a semi-infinite medium with either (a) a homogeneous semi-infinite source or (b) a depleting source (Crank 1975). The solution for the semi-infinite source [case (a)] always yielded better statistical fit to the experimental data than that for a depleting source [case (b)]. The fit to the experimental data according to the case (a) is illustrated in Fig. 1b. The data within the domain marked as SIMS instability were neglected in the fitting procedure. The semi-infinite source solution of the diffusion equation is (Crank 1975)

$$\frac{C_s - C(x, t)}{C_s - C_\infty} = \text{erf}\left(\frac{x}{2\sqrt{Dt}}\right) \quad (1)$$

where x is the normal distance from the interface, t is the time, C_s is the surface concentration and $C_\infty = C$ at $t = 0$. The surface concentration of the diffusing (and any other) species, C_s , could not be determined because of the typical instability of the SIMS analyses in the first four or five analytical cycles. Thus, as in our earlier studies (e.g. Ganguly et al. 1998a, 2007; Tirone et al. 2005), the solution to the diffusion equation was interfaced with an optimization program that yields the best combination of C_s and D values. Tirone et al. (2005) showed by Rutherford Back Scattering (RBS) measurement that a thin film of Nd indeed preserved the property of a homogeneous semi-infinite reservoir during diffusion into a garnet over a distance of 1,000 Å. Optimization analysis of the solutions to the SIMS data for the same sample also yielded better fit for a homogeneous semi-infinite source [case (a)] than a depleting source [case (b)].

The retrieved $D^*(\text{Ca})$ and $D^*(\text{Mg})$ data for the time series experiments at 1 bar, 1,000 °C, and $f(\text{O}_2)$ corresponding to the WI buffer condition that are mentioned above are illustrated in Fig. 2. The diffusion direction for these experiments is parallel to the b -axis of diopside. The

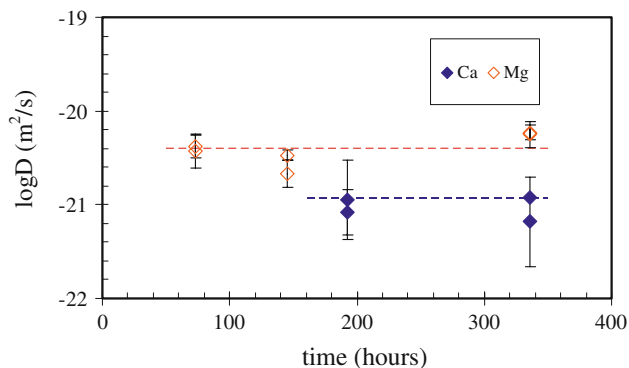


Fig. 2 Tracer diffusion coefficients of ^{44}Ca and ^{26}Mg parallel to the b axis of diopside retrieved from time series experiments at 1 bar, 1,000 °C and $f(\text{O}_2)$ corresponding to the WI buffer condition. Half-lengths of the vertical bars represent 2σ statistical errors

diffusion coefficients for both ^{44}Ca and ^{26}Mg do not show any noticeable dependence on time. Thus, there is no evidence for the interference of any non-diffusive process on the development of the concentration profiles of Ca and Mg in our experimental studies.

The experimental conditions and retrieved $D^*(^{44}\text{Ca})$ and $D^*(^{26}\text{Mg})$ values at different conditions along different crystallographic directions are summarized in Tables 1 and 2, respectively. There are two primary sources of statistical errors in the retrieved D values: (a) scatter of the data and (b) error in the measurement of crater depth. However, using the relation $D \propto x^2$, we find that the error of a D value ($\sim 1.5\%$ on the average) resulting from that of crater depth measurement is negligible compared to those arising from the scatter of the data points in a measured concentration profile. The latter was calculated according to the numerical method of Tirone et al. (2005) and was shown in Table 1 as $\pm 1\sigma$ values.

Arrhenian relations and diffusion anisotropy

Figures 3 and 4 show the Arrhenius plots of the experimentally determined diffusion parameters of ^{44}Ca and ^{26}Mg , respectively, as function of temperature along the a^* , b and c axial directions. The Arrhenian relation is expressed according to $D = D_0 \exp(-E/RT)$, where D_0 is a constant and E is the activation energy of diffusion. The vertical bars on the data points represent $\pm 2\sigma$ values.

The least squares fits to the $\log D$ versus $1/T$ data are illustrated in Figs. 3 and 4 as solid lines. The dashed lines show the 95% confidence intervals of the $\log D$ values that have been calculated according to the procedure of Tirone et al. (2005). The retrieved Arrhenian parameters are summarized in Table 3. The standard deviations of D_0 have been calculated from those of $\log D_0$, which are directly retrieved from the least squares regression of $\log D_0$ versus

Table 1 Summary of experimental conditions and ^{44}Ca tracer diffusion coefficients in diopside

Run#	T (°C)	Time (h)	$\log D(1\sigma)$ (m^2/s)	$D(1\sigma)$ (m^2/s)	$\text{Log}f\text{O}_2$ (bars)
Diffusion direction:// c -axis					
CaDi10c	1,150	24	−19.33 (± 0.10) −19.37 (± 0.04)	$4.68 (\pm 1.08) \times 10^{-20}$ $4.27 (\pm 0.43) \times 10^{-20}$	−12.14 (WI)
CaMgDi05c	1,100	48	−19.92 (± 0.08) −19.55 (± 0.06)	$1.20 (\pm 0.22) \times 10^{-20}$ $2.82 (\pm 0.39) \times 10^{-20}$	−12.9 (WI)
CaMgDi01c	1,050	72	−19.99 (± 0.06) −19.97 (± 0.06)	$1.02 (\pm 0.14) \times 10^{-20}$ $1.07 (\pm 0.15) \times 10^{-20}$	−14.42 (WI)
CaMgDi02	1,000	72	−20.39 (± 0.10) −20.41 (± 0.09)	$4.07 (\pm 0.94) \times 10^{-21}$ $3.89 (\pm 0.82) \times 10^{-21}$	−13.03 (WM)
CaDi11c	950	324	−20.82 (± 0.09) −21.18 (± 0.10)	$1.51 (\pm 0.32) \times 10^{-21}$ $6.61 (\pm 0.15) \times 10^{-22}$	−18.29 (WI)
Diffusion direction:// b -axis					
CaDi10b	1,150	24	−19.39 (± 0.06) −19.38 (± 0.10)	$4.07 (\pm 0.53) \times 10^{-20}$ $4.17 (\pm 1.00) \times 10^{-20}$	−12.14 (WI)
CaMgDi01b	1,050	72	−20.06 (± 0.06) −20.07 (± 0.06)	$8.71 (\pm 1.20) \times 10^{-21}$ $8.51 (\pm 1.18) \times 10^{-21}$	−14.42 (WI)
CaDi15b	1,000	192	−20.95 (± 0.24) −21.08 (± 0.08)	$1.11 (\pm 0.51) \times 10^{-21}$ $8.25 (\pm 2.10) \times 10^{-22}$	−16.19 (WI)
CaDi16b	1,000	336	−20.92 (± 0.16) −21.18 (± 0.07)	$1.22 (\pm 0.84) \times 10^{-21}$ $6.54 (\pm 1.41) \times 10^{-22}$	−16.19 (WI)
CaDi11b	950	324	−21.26 (± 0.13) −21.36 (± 0.04)	$5.50 (\pm 1.65) \times 10^{-22}$ $4.37 (\pm 0.44) \times 10^{-22}$	−18.29 (WI)
Diffusion direction:// a^* -axis					
CaDi10a	1,150	24	−19.49 (± 0.12) −19.44 (± 0.13)	$3.24 (\pm 0.91) \times 10^{-20}$ $3.63 (\pm 1.09) \times 10^{-20}$	−12.14 (WI)
CaMgDi01a	1,050	72	−20.12 (± 0.04) −20.24 (± 0.05)	$7.59 (\pm 0.76) \times 10^{-21}$ $5.75 (\pm 0.69) \times 10^{-21}$	−14.42 (WI)
CaDi11a	950	324	−21.36 (± 0.05) −21.38 (± 0.03)	$4.37 (\pm 0.48) \times 10^{-22}$ $4.17 (\pm 0.25) \times 10^{-22}$	−18.29 (WI)

The parenthetical numbers beside $\log f(\text{O}_2)$ indicate corresponding solid oxygen buffer conditions

$1/T$ data, according to $\sigma(D_0) = (2.303D_0) \times \sigma(\log D_0)$ (Liermann and Ganguly 2002). The Arrhenian relation for $D(^{44}\text{Ca})$ and $D(^{26}\text{Mg})$ parallel to the three axial directions are compiled in the lower right panels of Figs. 3 and 4, respectively.

It is evident from the illustrations of the diffusion data that both Ca and Mg diffusion are significantly anisotropic within the temperature range (950–1,150 °C) of the experimental data. According to the empirical relation known as the “compensation law”, $\log D$ versus $1/T$ relations within a given mineral should converge with increasing temperature so that at some high temperature, usually referred to as the “compensation temperature”, all diffusivities in a given crystal (or of a given species in different crystals) become the same (Winchell 1969; Lasaga 1998). The behavior of the $\log D$ versus $1/T$ relations for Ca diffusion parallel to a^* , b and c axial directions (Fig. 3) conforms to that expected from the “compensation law”. However, the $D^*(\text{Mg})$

values do not conform to the “compensation” behavior (Fig. 4). There are insufficient data in the literature to test if the “compensation law” holds at a statistically significant level for anisotropic diffusion.

Figure 5 shows a compilation of the Arrhenian relations for ^{44}Ca parallel to a^* , b and c and for ^{26}Mg parallel to b and c axial directions of diopside. It is interesting to find that these five relations seem to satisfy the “compensation relation” with a compensation condition defined by $\log D \approx -19.3 \text{ m}^2/\text{s}$, $T \approx 1,155 \text{ °C}$ (1,428 K). It, therefore, seems reasonable to suppose that the ^{26}Mg diffusion in diopside parallel to a^* should also satisfy the compensation relation. We, therefore, regress these data in diopside using the form of Arrhenian relation and constraining it to pass through the compensation condition. This is shown in Fig. 5 as “Mg($//a^*$): comp”, and the constrained Arrhenian parameters are listed in Table 3. We recommend these parameters for $D^*(^{26}\text{Mg})$ in diopside. The inset in Fig. 5

Table 2 Summary of experimental conditions and ^{26}Mg tracer diffusion coefficients in diopside

Run#	T ($^{\circ}\text{C}$)	Time (h)	$\log D(1\sigma)(\text{m}^2/\text{s})$	$D(1\sigma)(\text{m}^2/\text{s})$	$\text{Log}f\text{O}_2$ (bars)
Diffusion direction:// c -axis					
MgDi10c	1,150	24	−19.26 (± 0.03) −19.44 (± 0.06)	$5.50 (\pm 0.44) \times 10^{-20}$ $3.63 (\pm 0.47) \times 10^{-20}$	−12.14 (WI)
CaMgDi05c	1,100	48	−19.64 (± 0.08) −19.39 (± 0.08)	$2.29 (\pm 0.42) \times 10^{-20}$ $4.07 (\pm 0.75) \times 10^{-20}$	−12.90 (WI)
CaMgDi01c	1,050	72	−19.82 (± 0.05) −19.78 (± 0.08)	$1.51 (\pm 0.17) \times 10^{-20}$ $1.66 (\pm 0.30) \times 10^{-20}$	−14.42 (WI)
CaMgDi02	1,000	72	−19.97 (± 0.06) −19.91 (± 0.07)	$1.07 (\pm 0.14) \times 10^{-20}$ $1.23 (\pm 0.20) \times 10^{-20}$	−13.03 (WM)
MgDi11c	950	324	−20.48 (± 0.04) −20.42 (± 0.07)	$3.32 (\pm 0.30) \times 10^{-21}$ $3.80 (\pm 0.61) \times 10^{-21}$	−18.29 (WI)
Diffusion direction:// b -axis					
MgDi10b	1,150	24	−19.50 (± 0.14) −19.38 (± 0.10)	$3.16 (\pm 1.01) \times 10^{-20}$ $4.17 (\pm 1.00) \times 10^{-20}$	−12.14 (WI)
CaMgDi01b	1,050	72	−19.87 (± 0.09) −19.88 (± 0.09)	$1.34 (\pm 0.28) \times 10^{-20}$ $1.31 (\pm 0.27) \times 10^{-20}$	−14.42 (WI)
MgDi12b	1,000	73	−20.38 (± 0.06) −20.43 (± 0.09)	$4.17 (\pm 0.54) \times 10^{-21}$ $3.72 (\pm 0.78) \times 10^{-21}$	−16.19 (WI)
MgDi13b	1,000	145	−20.47 (± 0.03) −20.67 (± 0.07)	$3.39 (\pm 0.24) \times 10^{-21}$ $2.14 (\pm 0.34) \times 10^{-21}$	−16.19 (WI)
MgDi15b	1,000	336	−20.23 (± 0.04) −20.25 (± 0.07)	$5.93 (\pm 0.58) \times 10^{-21}$ $5.63 (\pm 1.75) \times 10^{-21}$	−16.19 (WI)
MgDi11b	950	324	−20.90 (± 0.04) −20.66 (± 0.09)	$1.26 (\pm 0.08) \times 10^{-21}$ $2.19 (\pm 0.44) \times 10^{-21}$	−18.29 (WI)
Diffusion direction :// a^* -axis					
MgDi10a	1,150	24	−19.71 (± 0.07) −19.56 (± 0.06)	$1.95 (\pm 0.33) \times 10^{-20}$ $2.75 (\pm 0.39) \times 10^{-20}$	−12.14 (WI)
CaMgDi01a	1,050	72	−20.06 (± 0.07) −20.15 (± 0.07)	$8.71 (\pm 1.39) \times 10^{-21}$ $7.08 (\pm 1.13) \times 10^{-21}$	−14.42 (WI)
MgDi11a	950	324	−20.57 (± 0.09) −20.50 (± 0.10)	$2.69 (\pm 0.54) \times 10^{-21}$ $3.16 (\pm 0.70) \times 10^{-21}$	−18.29 (WI)

The parenthetical numbers beside $\log f(\text{O}_2)$ indicate corresponding solid buffer conditions

shows a comparison of the constrained Arrhenius relation with the experimental data of Mg diffusion parallel to the a^* axis.

Modeling of compositional zoning in the exsolved (001) augite lamellae in clinopyroxene requires diffusion data normal to the lamellar surface. This normal direction makes an angle of 16° – 18° with the c axis of augite. Considering the difference between the D values parallel to a^* and c axial directions, and the errors in the retrieved D values, we feel that a linear interpolation of D value as a function of angle with respect to an axial direction in the a – c plane should be adequate to define D normal to (001). This approximation does not yield any significant difference between D (\perp (001) and D (// c).

In principle, the diffusion coefficient along any arbitrary direction, x , can be determined if the diffusion coefficients

along the three principal axes of diffusion and the direction cosines of x with respect to these axes are known (e.g. Crank 1975). Since an axis of symmetry constitutes a principal axis, the D (// b) yields the diffusion coefficient parallel to one of the principal axes. More work (i.e. determination of D parallel to at least one more direction in the a – c plane) is needed to define the other two principal axes and diffusion coefficients parallel to these axes. The general mathematical procedures are discussed by Nye (1985).

Chemical interdiffusion coefficient of Ca and Mg in diopside

A binary chemical inter-diffusion coefficient between two species i and j is related to the individual self-diffusion

Fig. 3 Arrhenius plot of the tracer diffusion coefficients of ^{44}Ca parallel to the a^* , b and c axial directions of diopside at $f(\text{O}_2)$ corresponding to the WI buffer condition. The *solid lines* are least squares fits to the experimental data. The *vertical bars* on the data points represent $\pm 2\sigma$ error, and the *dashed curves* show the $\pm 95\%$ error envelopes of the regressed relations. The *lower right panel* shows a comparison of the Arrhenian relations for diffusion parallel to a^* , b and c directions

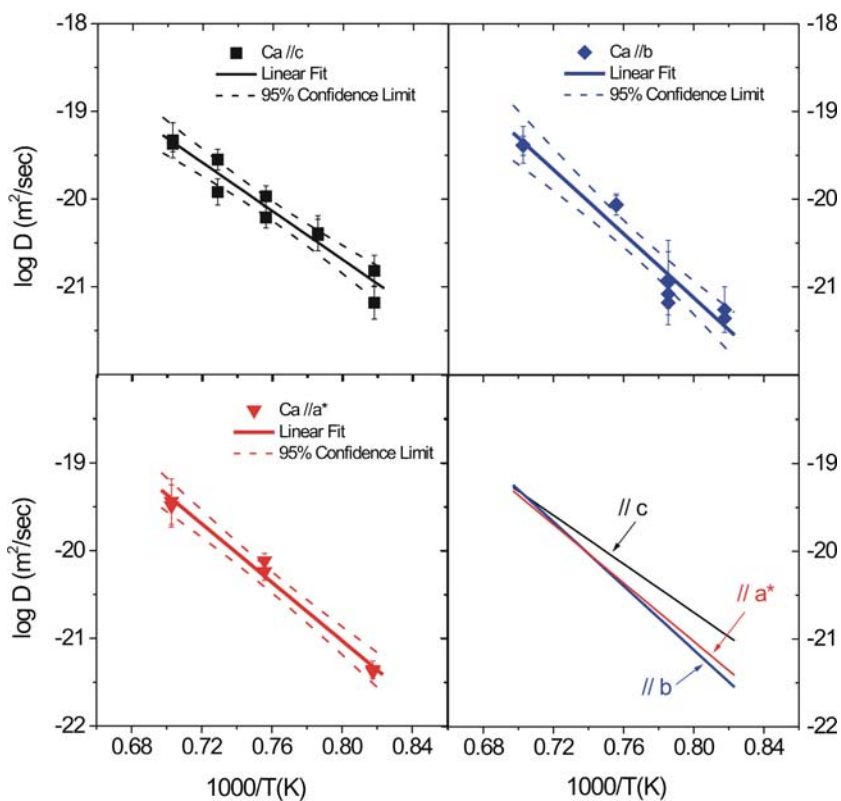


Fig. 4 Same as Fig. 3 for ^{26}Mg diffusion

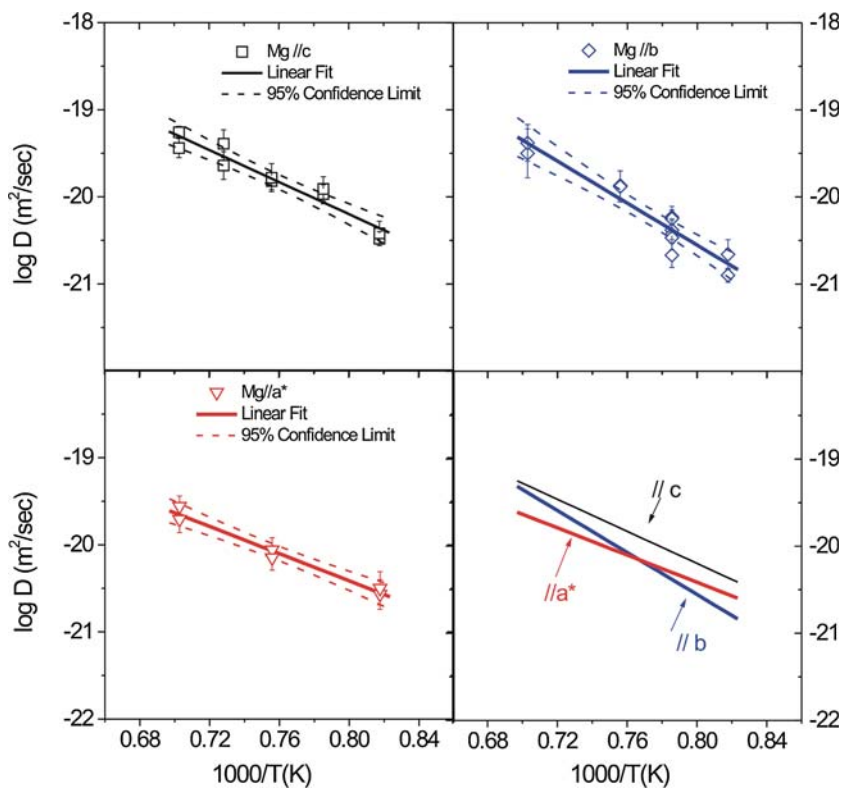


Table 3 Summary of ⁴⁴Ca and ²⁶Mg diffusion parameters in diopside

//a*	//b	//c
Ca		
logD* ₀ (m ² /s)		
-7.7 (0.7)	-6.52 (1.29)	-9.62 (0.91)
D* ₀ × 10 ⁹ (m ² /s)		
19.9 (32.2)	302.0 (897.0)	0.24 (0.50)
E (kJ/mol-K)		
318.80 (17.68)	349.50 (32.06)	264.96 (22.99)
Mg		
logD* ₀ (m ² /s)		
-14.17 (0.49)	-10.91 (0.93)	-12.84 (0.68)
D* ₀ × 1,0 ¹³ (m ² /s)		
0.07 (0.08)	123.0 (263.0)	1.44 (2.26)
E (kJ/mol-K)		
149.50 (22.24)	230.69 (22.92)	176.15 (176)
Mg://a* constrained to obey compensation law		
logD* ₀ (m ² /s) = -11.39 (1.19) [D* ₀ (m ² /s) = 4.07 (11.16) × 10 ⁻¹²]		
E (kJ/mol-K) = 218.08 (15.93)		

The parenthetical numbers represent 1σ values

coefficients, D(i), according to (e.g. Brady and McCallister 1983; Ganguly 2002)

$$D(i-j) = \frac{D(i)D(j)}{X_iD(i) + X_jD(j)} \left(1 + \frac{\partial \ln \gamma_i}{\partial \ln X_i} \right) \quad (2)$$

where γ_i is the thermodynamic activity coefficient of the species i. The tracer diffusion coefficient of an isotope of an element and the self diffusion coefficient are equivalent when all isotopes of the element have the same diffusivities. The concepts of tracer, self and chemical diffusion coefficients have been reviewed and discussed by Ganguly (2002). Assuming that the self and tracer diffusion coefficients of Ca and Mg are effectively the same, the above relation can be used to calculate D(Ca–Mg). The parenthetical term in this equation is usually referred to as the thermodynamic factor (TF). Brady and McCallister (1983) demonstrated that there is a strong influence of TF on D(Ca–Mg) in diopside that results from large deviation from ideality of mixing of these species, which is manifested in the presence of a large solvus in the binary system.

To calculate the dependence of D(Ca–Mg) on the composition of diopside, we use the Ca–Mg mixing parameters from Lindsley et al. (1981). These authors modeled the molar excess free energy of mixing, ΔG_m^{xs}, in the Ca–Mg binary join in terms of a sub-regular model

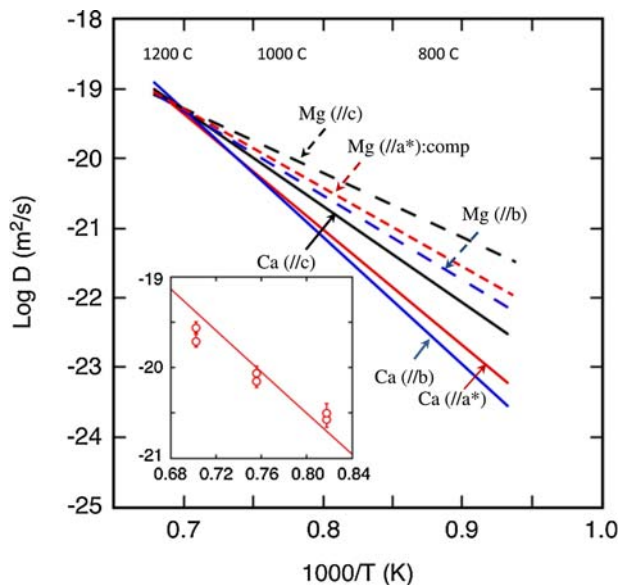


Fig. 5 Comparison of the Arrhenian relations of ⁴⁴Ca and ²⁶Mg tracer diffusivities parallel to the a*, b and c axial directions of diopside at f(O₂) corresponding to the WI buffer. The dashed line labeled “Mg(//a*): comp” shows the Arrhenian relation for Mg diffusion parallel to a*, constrained to satisfy the compensation condition defined by the others. The inset shows a comparison of the constrained Arrhenius relation with the experimental data for diffusion of Mg parallel to the a* axis

$$\Delta G_m^{xs} = (W_{MgCa}X_{Ca} + W_{CaMg}X_{Mg})X_{Ca}X_{Mg} \quad (3)$$

that yields

$$RT \ln \gamma_i = [W_{ij} + 2X_i(W_{ji} - W_{ij})]X_j^2 \quad (4)$$

(e.g. Ganguly and Saxena 1987), where the W parameters are subregular fitting parameters that are, in principle, functions of pressure and temperature, but not composition. From the last expression, we obtain

$$TF \equiv \left(1 + \frac{\partial \ln \gamma_i}{\partial \ln X_i} \right) = \frac{X_i X_j}{RT} [W_{ij}(2X_i - 4X_j) + W_{ji}(2X_j - 4X_i)]. \quad (5)$$

According to Lindsley et al. (1981) W_{CaMg} = 31,217 + 0.0061(P) J/mol and W_{MgCa} = 25,485 + 0.0812(P) J/mol where P is in bars. Figure 6 shows the thermodynamic factor versus mol fraction of diopside in the Ca–Mg binary join at 1,200, 1,000 and 800 °C and pressure of 1 bar (solid lines) and at 1,200 °C, 10 kb (dashed line).

Figure 7 shows the Arrhenius relations of D(Ca–Mg) for X(Di) of 0.8 and 0.9 to illustrate the effect of the thermodynamic factor on the interdiffusion coefficient. The Arrhenius relations for ideal mixing at the two compositions are indistinguishable in the graph, and are thus shown by a single dashed line. The activation energy value is 223.7 kJ/mol for ideal mixing, and after including the

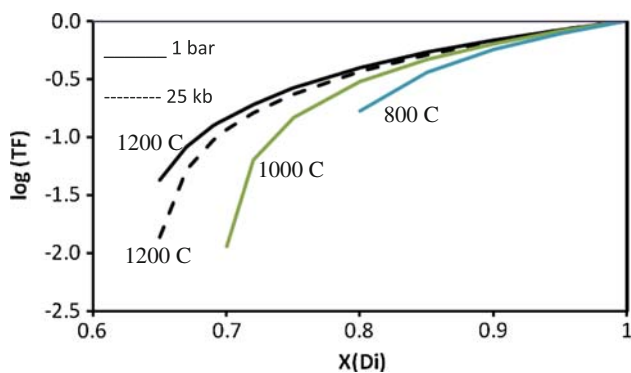


Fig. 6 Illustration of the (non-coherent) thermodynamic factor of chemical diffusion coefficient in diopside-clinoenstatite ($\text{CaMgSi}_2\text{O}_6\text{--MgMgSi}_2\text{O}_6$) binary as function of the mole fraction of diopside at 1,200, 1,000 and 800 °C, 1 bar (solid lines) and 1,200 °C, 10 kb (dashed line). The calculations terminate at the solvus

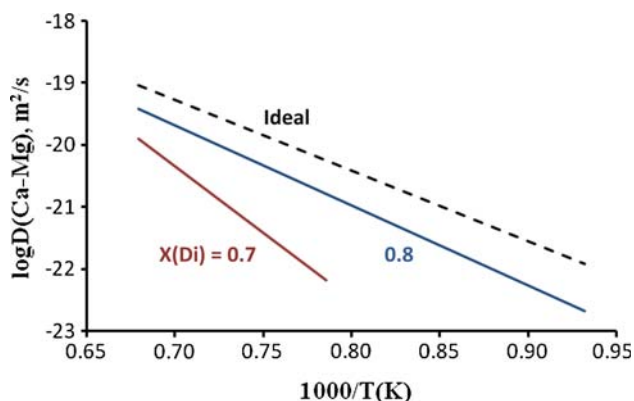


Fig. 7 Arrhenius relations of Ca-Mg interdiffusion coefficient as function of composition, with and without thermodynamic effects. The solid lines show the Arrhenius relations for $X(\text{Di}) = 0.7$ and 0.8 . The Arrhenius relations for ideal mixing in these compositions are indistinguishable in the graph, and shown by a dashed line

thermodynamic effect, 427.4 and 251.9 kJ/mol for $X(\text{Di}) = 0.7$ and 0.8 , respectively.

Comparison with previous studies

Figure 8 shows a comparison of tracer diffusion data parallel to the c axis for ^{44}Ca and ^{26}Mg , as determined in this study, with those of Ca and Fe^{2+} of Dimanov et al. (1996) and Azough and Freer (2000), respectively, and Ca-(Mg + Fe) quasibinary chemical inter-diffusion data normal to (001) by Brady and McCallister (1983) and Fujino et al. (1990). Dimanov et al. (1996) also carried out a limited number of experiments for diffusion parallel to the b axis at 1,180–1,250 °C, but did not find any significant difference between the diffusion data parallel to the b and c axial directions. This observation about the similarity of $D(\text{Ca})//b$ and $D(\text{Ca})//c$ is consistent with our finding that

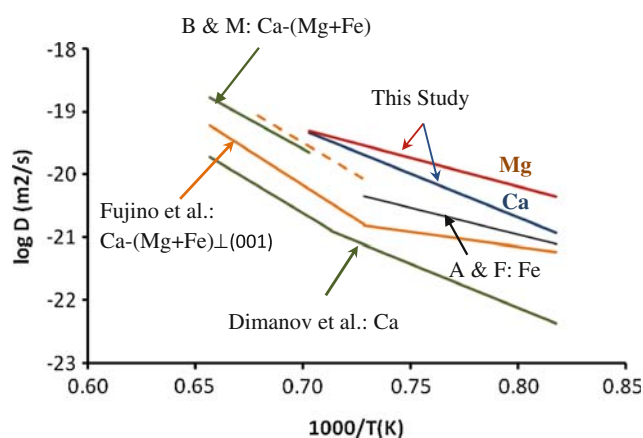


Fig. 8 Comparison of diffusion data parallel or approximately parallel to c -axis in diopside. *B & M* Brady and McCallister (1983); *A & F* Azough and Freer (2000). The dashed line represents the calculated $D(\text{Ca--Mg})$ for the average $X(\text{Di})$ composition in the experiments of Fujino et al. (1990). All data are at 1 bar, except for Brady and McCallister (1983), which are at 25 kb. The data of Fujino et al. (1990) and Brady and McCallister (1983) are normal to (001) (i.e. inclined by 16–18° to the c -axis)

the diffusion anisotropy of Ca in diopside almost vanishes at $\sim 1,150$ °C (Fig. 3). Because of the lack of difference between their data for $D(\text{Ca})$ parallel to the b and c axial directions, Dimanov et al. (1996) fitted all their data (71 D values// c and 6 D values// b) with a single Arrhenian relation. We find that while the activation energy of Ca diffusion parallel to the c axis, as determined in this study, is similar to that in Dimanov et al. (1996), the $D(\text{Ca})$ values of this study are 1.0–1.5 log units larger. There is also a slight kink in the $\log D(\text{Ca})$ versus $1/T$ relation presented by Dimanov et al., but there does not seem to be any statistical justification for such a kink considering the scatter of their experimental data.

The quasibinary Ca-(Mg + Fe) chemical interdiffusion data of Fujino et al. (1990) show a conspicuous change of slope in the Arrhenius plot (Fig. 7) that suggests a change of diffusion mechanism. This is in contrast to our data that do not suggest any change of slope of the $\log D$ versus $1/T$ relation. We also note that intrinsic-extrinsic transition that was suggested earlier for Fe-Mg interdiffusion in olivine (Buening and Buseck 1973) is not supported by a thorough investigation of the problem by Chakarabarty and co-workers for over more than a decade, the results of which are summarized in Dohmen and Chakarabarty (2007), nor was such a transition found within the temperature range of 750–1,450 °C for Mg tracer diffusion in garnet (Ganguly et al. 1998b) and in many other modern studies of cation diffusion in silicates and oxides. Although used by several workers for modeling compositional zoning in pyroxenes to retrieve the time scales of natural processes (e.g. Miyamoto and Takeda 1994), the data of Fujino et al.

(1990) have not been available in any peer reviewed international journal. Therefore, it is not possible to provide a critical evaluation of these diffusion data.

In order to roughly compare the chemical Ca–(Mg + Fe) inter-diffusion data of Fujino et al. (1990) and Brady and McCallister (1983) with our results, we need to calculate the Ca–Mg binary diffusion normal to the (001) lamellae from our data, incorporating the effects of the thermodynamic factor (TF). The comparison with the data of Brady and McCallister (1983) also requires that we calculate the effect of pressure on diffusion coefficient as their experiments were carried out at 25 kb. As noted above, there is no significant difference between $D(\parallel c)$ and $D(\perp(001))$ if it is assumed that D changes linearly as function of angle with respect to an axial direction in the a – c plane between the values parallel to c and a^* directions.

The average diopside content of the augite host in the experiments of Fujino et al. (1990) is found to be ~81 mol% at 1,100 °C and 74 mol% at 1,200 °C (Fujino, pers. com.). Thus, using Eq. 5 and the thermodynamic mixing parameters of Lindsley et al. (1981), we calculate $\log(\text{TF}) = -0.47$ and -0.55 at 1,100 °C and 1200 °C, respectively, at $P = 1$ bar. From Eq. 2, we then calculate $D(\text{Ca–Mg})$ at 1 bar, 1,100 and 1,200 °C. The linear $\log D(\text{Ca–Mg})$ versus $1/T$ relation defined by these data are illustrated in Fig. 8 by a dashed line. The calculated $D(\text{Ca–Mg})$ values are ~0.6–0.7 log unit greater than the experimental quasibinary $D(\text{Ca–(Fe + Mg)})$ data of Fujino et al. (1990). A part of this difference may be due to the presence of Fe ($\text{Fe}/\Sigma\text{M-cations} \sim 0.13$) in the sample used by Fujino et al. (1990). Comparison of our data with those of Azough and Freer (2000) suggests that $D(\text{Fe})$ is the slowest diffusing divalent cation in diopside. It is, however, doubtful if $D(\text{Fe}) < D(\text{Ca})$ as the ionic radius of Ca is much larger than that of Fe^{2+} . It seems more likely that $D(\text{Fe})$ is smaller than $D(\text{Mg})$, as has been shown to be the case for Mn poor garnet (Ganguly et al. 1998b), but greater than $D(\text{Ca})$.

At a constant temperature, the pressure dependence of a diffusion coefficient is given by the relation

$$\frac{\partial \log D}{\partial P} = -\frac{\Delta V^+}{2.303RT} \quad (6)$$

where ΔV^+ is the activation volume. No data are, however, yet available for the ΔV^+ (Ca–Mg) for clinopyroxene. Theoretical analysis of the problem of estimation of activation volume by Sammis et al. (1981) suggests that in a given mineral group, the ratio of $\Delta V^+/E$ should be approximately constant. The experimental data for Ce and Yb diffusion in diopside by Van Orman et al. (2001) yields $\Delta V^+/E = 0.022$ – 0.023 cm^3/kJ . Thus, using the E values for Ca and Mg diffusion parallel to the c -axis, as determined in this study, we obtain ΔV^+ (Ca) ~6 cm^3/mol and ΔV^+ (Mg) ~4 cm^3/mol , and consequently, using Eq. 6,

$\Delta \log D = -0.55$ for Ca and -0.37 for Mg diffusion parallel to the c -axis in diopside at 1,150 °C, where Δ stands for the change of $\log D$ value for an increase of pressure from 1 bar to 25 kb. The estimated activation volumes are comparable to those determined experimentally for Mg, Fe^{2+} , Mn^{2+} diffusion in garnet (Chakraborty and Ganguly 1992) and olivine (Holzapfel et al. 2007).

The average composition of augite during the homogenization experiment at 25 kb, 1,150 °C, as reported by Brady and McCallister (1983), has ~73 mol% diopside component. Since the experimental studies involved homogenization of coherent (001) pigeonite exsolution lamellae, the thermodynamic factor should be calculated, as pointed out by Brady and McCallister (1983), on the basis of the mixing parameters describing the coherent solvus. From the calculations of thermodynamic factor presented by these workers, we find $\log(\text{TF}) \approx -0.6$. Thus, at 25 kb, 1,150 °C, our tracer diffusion data yield, after incorporating pressure and thermodynamic effects, $\log D(\text{Ca–Mg}) = -20.3$ m^2/s , as compared to -19.7 m^2/s that was determined by Brady and McCallister (1983) from lamellar homogenization experiments.

Cooling rates of non-cumulate eucrites: a test of the diffusion data

Because of the disagreement among the various sets of data, selection of the most correct data set may have to be made by comparison of their consequences against other constraints. To this end, we compare the cooling rates of eucrites calculated by Schwartz and McCallum (2005) from lamellar coarsening kinetics with those calculated from the compositional zoning within the host–lamellae pairs using Ca–Mg diffusion data. Using the theory of Brady (1987) on lamellar coarsening kinetics and the experimental data of coarsening kinetics by Nord and McCallister (1979) and Nord and Gordon (1980), Schwartz and McCallum (2005) derived cooling rates of 10^{-2} °C/day and $3(10^{-5})$ °C/day for the attainment of the observed lamellar thicknesses in two planetary basaltic samples, known as Pasamonte and Haraiya, respectively. These are non-cumulate basaltic materials (eucrite) that are generally believed to have been derived from the asteroid Vesta. Schwartz and McCallum (2005) have also determined the maximum cooling rates for these samples on the basis of the observed compositional zoning within the host–lamellae pairs in these eucrites, using the preliminary Ca and Mg tracer diffusion data from our group (Stimpfl et al. 2003), and assuming constant cooling rate. The results are 10^{-2} °C/day for Pasamonte and 10^{-4} °C/day for Haraiya.

The initial cooling rate of a system is independent of the cooling model (Ganguly et al. 1994). Also, the cooling rate

derived from one set of diffusion data can be adjusted to yield cooling rate corresponding to a different set of data by noting that the integral quantity $\int D(t)dt$ is invariant (the explicit functional dependence of D on t depends on the T - t relation), as long as the initial and boundary conditions are the same. Thus, extending the treatment of the cooling rate problem by Ganguly et al. (1994), it can be easily shown that the initial cooling rates (\dot{T}) derived from the application of two different sets of diffusion data to the same compositional profile are related according to

$$\frac{\dot{T}_1}{\dot{T}_2} = \frac{D_1(T_0)/D_2(T_0)}{E_1/E_2} \quad (7)$$

where $D_i(T_0)$ is the diffusion coefficient at T_0 according to the data set i .

The thermodynamically corrected chemical inter-diffusion data for the augite lamella in the eucrites, as calculated from our tracer diffusion data and the thermodynamic mixing properties of Ca and Mg given by Lindsley et al. (1981), yields an Arrhenian relation of $D(\text{Ca-Mg}) = 4(10^{-12})\exp(-E/RT)$ m²/s with $E = 218,143$ J/mol. Schwartz and McCallum (2005) assumed an initial temperature of 1,100 °C. Using these data, we obtain from the last equation \dot{T} (this study)/ \dot{T} (S & M) = 3.22. Thus, our diffusion data yield initial cooling rates of $\leq 3(10^{-3})$ °C/day and $\leq 3(10^{-5})$ °C/day for Pasamonte and Hariya, respectively. Modeling of lamellar coarsening yields a factor of three faster cooling rate for Pasamonte and the same cooling rate for Hariya. All other diffusion data at one bar (Fig. 8) would yield cooling rates that are much slower than those obtained from the lamellar coarsening kinetics.

Acknowledgments This research was supported by a grant from the NASA Cosmochemistry program NNX07AJ74G. We are grateful to Prof. N. Sugiura and Dr. Miyazaki for providing access to the SIMS facility at the University of Tokyo while M.I. has been at the same University on a JSPS fellowship, and to Prof. Richard Hervig for providing access to the SIMS facility at the Arizona State University and helpful advice on the analytical procedures. Our sincere thanks are due to Profs. Youxue Zhang and Jim Van Orman for constructive reviews of the manuscript, and to Prof. Rabi Bhattacharya for deriving the relation for constrained regression for Mg diffusion. We also thank Dr. Marilena Stimpfl for some of the initial studies that have partly laid the groundwork of the experimental investigations.

References

- Azough F, Freer R (2000) Iron diffusion in single-crystal diopside. *Phys Chem Minerals* 27:732–740
- Brady JB (1987) Coarsening of fine-scale exsolution lamellae. *Am Min* 72:697–706
- Brady JB, McCallister RH (1983) Diffusion data for clinopyroxenes from homogenization and self-diffusion experiments. *Am Min* 68:95–105
- Buening DK, Buseck PR (1973) Fe–Mg lattice diffusion in olivine. *J Geophys Res* 78:6861–68521
- Chakraborty S, Ganguly J (1992) Cation diffusion in aluminosilicate garnets: experimental determination in spessartine-almandine diffusion couples, evaluation of effective binary diffusion coefficients, and applications. *Contrib Mineral Petrol* 111:74–86
- Crank J (1975) *The mathematics of diffusion*, 2nd edn. Clarendon Press, Oxford
- Dimanov A, Jaoul O, Sautter V (1996) Calcium self-diffusion in natural diopside crystals. *Geochim Cosmochim Acta* 60:4095–4106
- Dohmen R, Chakraborty S (2007) Fe–Mg diffusion in olivine II: point defect chemistry, change of diffusion mechanisms and a model for calculation of diffusion coefficients in natural olivine. *Phys Chem Minerals* 34:409–430
- Fujino K, Nachara H, Momoi H (1990) Direct determination of cation diffusion coefficients in pyroxenes. *EoS Trans Am Geophys Union* 71:943–944
- Ganguly J (2002) Diffusion kinetics in minerals: principles and applications to tectono-metamorphic processes. In: Gramaccioli CM (ed) *Energy modelling in minerals*. EMU Notes in Mineralogy, vol 4, pp 271–309
- Ganguly J, Saxena SK (1987) *Mixtures and mineral reactions*. Springer, Berlin, p 291
- Ganguly J, Yang H, Ghose S (1994) Thermal history of mesosiderites: quantitative constraints from compositional zoning and Fe–Mg ordering in orthopyroxenes. *Geochim Cosmochim Acta* 58:2711–2723
- Ganguly J, Tirone M, Hervig RL (1998a) Diffusion kinetics of Samarium and Neodymium in garnet, and a method for determining cooling rates of rocks. *Science* 281:805–807
- Ganguly J, Cheng W, Chakraborty W (1998b) Cation diffusion in aluminosilicate garnets: experimental determination in pyrope-almandine diffusion couples. *Contrib Mineral Petrol* 131:171–180
- Ganguly J, Ito M, Zhang X-Y (2007) Cr diffusion in orthopyroxene: Experimental determination, ⁵³Mn–⁵³Cr thermochronology, and planetary applications. *Geochim Cosmochim Acta* 71:3915–3925
- Holzappel C, Chakraborty S, Rubie DC, Frost DJ (2007) Effect of pressure on Fe–Mg, Ni and Mn diffusion in (Fe_xMg_{1-x})₂SiO₄ olivine. *Phys Earth Planet Int* 162:186–198
- Lasaga SC (1998) *Kinetic theory in earth sciences*. Princeton, p 811
- Liermann P, Ganguly J (2002) Diffusion kinetics of Fe²⁺ and Mg in aluminous spinel: Experimental determination and applications. *Geochim Cosmochim Acta* 66:2903–2913
- Lindsley DH, Grover JE, Davidson PM (1981) The thermodynamics of the Mg₂Si₂O₆–CaMgSi₂O₆ join: a review and a new model. In: Newton RC, Navrotsky A, Wood BJ (eds) *Advances in physical Geochemistry*, vol 1. Springer, Berlin, pp 149–175
- McCallister RH (1978) The coarsening kinetics associated with exsolution in an iron-free pigeonite. *Contrib Mineral Petrol* 65:327–331
- McCallum IS, O'Brien HE (1996) The stratigraphy of lunar highland crust: depths of burial of lunar samples from cooling rate studies. *Am Min* 81:1166–1175
- Miyamoto M (1997) Chemical zoning of olivine in several pallasites. *J Geophys Res* 102:21613–21618
- Miyamoto M, Takeda H (1994) Evidence for excavation of deep crustal material for a Vesta-like body from Ca compositional gradients in pyroxene. *Earth Planet Sci Lett* 122:343–349
- Nord GL, Gordon L (1980) Decomposition kinetics in clinopyroxenes. *GSA Abst Prog* 12:492
- Nord GL, McCallister RH (1979) Kinetics and mechanism of decomposition in Wo₂₅En₃₁Fs₄₄ clinopyroxene. *GSA Abst Prog* 11:488
- Nye JF (1985) *Physical properties of crystals: their representation by tensors and matrices*. Oxford, p 329

- Sammis CG, Smith JC, Schubert G (1981) A critical assessment of estimation methods for activation volume. *J Geophys Res* 86:10707–10718
- Schwartz JM, McCallum IS (2005) Comparative study of equilibrated and unequilibrated eucrites: subsolidus thermal histories of Haraiya and Pasamonte. *Am Min* 90:1871–1886
- Stimpfl M, Ganguly J, Hervig R (2003) Ca and Mg tracer diffusion in diopside: experimental determination and applications to cooling history of planetary samples. In: Lunar planet science conference XXXIV
- Tirone M, Ganguly J, Dohmen R, Langenhorst F, Hervig R, Becker H-W (2005) Rare earth diffusion kinetics in garnet: experimental studies and applications. *Geochim Cosmochim Acta* 69:2385–2398
- Van Orman JA, Grobe TL, Schimizu N (2001) Rare earth element diffusion in diopside: influence of temperature, pressure and ionic radius, and an elastic model for diffusion in silicates. *Contrib Mineral Petrol* 141:687–703
- Winchell P (1969) The compensation law for diffusion in silicates. *High Temp Sci* 1:200–215